This is an Accepted Manuscript of an article published in the Journal of Hydrologic Engineering in 2010, available online: doi:10.1061/(ASCE)HE.1943-5584.0000161

Comparison of Flood Top Width Predictions using Surveyed and LiDAR-Derived Channel Geometries

Fadi M. Shatnawi, M. ASCE[1] and Jonathan L. Goodall, M. ASCE[2]

Abstract

This paper compares flood top width predictions generated by a 1-D flood model (HEC-RAS) using surveyed and LiDAR-based topographic descriptions for varying storm event return intervals. Three channel geometries are used in the analysis: (1) based entirely on survey data, (2) based entirely on LiDAR data and (3) based on a hybrid file that merges survey-derived channel bank locations and LiDAR-derived cross sections. The study area is a 6.6-km river reach located in the Piedmont area of North Carolina. Four steady flow simulations are performed representing the 10-year, 50-year, 100-year and 500-year design storm events to understand the effect of storm return period on top width predictions using the three different topographic descriptions. The results from the study suggest that the LiDAR derived geometries generally predicted higher widths compared to the survey geometries, and that the magnitude of the difference is inversely related to the storm even return interval (12% average difference for a 10-year storm event to 4% for a 500-year storm event).

Subject Headings: Floods; Mapping; Terrain models; Hydraulic modeling; Geographic information systems

[1] Graduate Research Assistant, Department of Civil and Environmental Engineering, University of South Carolina, 300 Main Street, Columbia, South Carolina 29208, fmshatna@engr.sc.edu

[2] Assistant Professor, Department of Civil and Environmental Engineering, University of South Carolina, 300 Main Street, Columbia, South Carolina 29208, goodall@engr.sc.edu

Introduction

Extreme flood events are a major natural hazard that affects communities worldwide. Flooding threats are likely to increase given climate change predictions that suggest higher sea levels and more intense cyclonic weather systems and precipitation (IPCC 2001). Several studies have shown that the frequency, distribution, and causes of floods over the last thirty years have increased in several areas of the world, including several areas in the United States (WMO 2003). Mitigation of flood losses requires accurate and current floodplain maps. However, floodplain maps and management studies have been expensive to produce and keep up-to-date. In addition, modeling of channels and floodplain geometry has traditionally been performed using survey data that is time consuming to gather. Today, new technologies such as GIS, GPS, and remote sensing are helping floodplain managers to create accurate and current floodplain maps with improved efficiency and speed, and at a reasonable cost (NAS 2007; Shamsi 2001).

In 1997, the Federal Emergency Management Agency (FEMA) initiated the Map Modernization Program to update their database of approximately 100,000 Flood Insurance Rate Maps (FIRMs). After the massive 1999 flood caused by Hurricane Floyd in eastern North Carolina, critical weaknesses were identified in the rescue, recovery, and mitigation efforts of the flood (USACE and FEMA 2000). Two weaknesses identified were (1) that the original FIRMs only delineate the 100-year event and (2) that the FIRMs were out of date and of limited utility during the flood. As a response to the Map Modernization Program effort and the aftermath of Hurricane Floyd, the State of North Carolina, with the support of FEMA, undertook the North Carolina Floodplain Mapping Program (NCFMP 2003). A major component of the NCFMP was the development and completion of statewide LiDAR (Light Detection and Ranging) Digital Elevation Model (DEM) at 6.1-m (20-ft) horizontal resolution. These topographic data are used with other digital information and field data to analyze flood hazards and delineate floodplain boundaries, which are depicted on Flood Insurance Rate Maps (DFIRMs) (FEMA 2003; NCFPM 2003).

The process of creating flood maps involves both hydrology and hydraulic modeling. A common model used for the hydraulic portion of the analysis is the U.S. Army Corps. of Engineers' River Analysis System (HEC-RAS). HEC-RAS is capable of performing three types of one-dimensional hydraulic analyses: (1) steady flow water surface profile computations, (2) unsteady flow simulation, and (3) movable boundary sediment transport computations. A key element is that all three analyses use a common geometric data representation and common geometric and hydraulic computation routines. HEC-RAS is well tested and well suited to the applications necessary for flood mapping, it is freely available, and it is approved by FEMA. For these reasons, it was the hydraulic model used in this study.

The availability of high resolution digital elevation data through LiDAR instrumentation has the potential to provide an automated means for generating the channel cross section geometry files required by HEC-RAS. However, while studies have quantified errors in cross sections generated by LiDAR, (Walker and Willgoose, 1999) or in flood inundation for single flow events (Wang and Zheng, 2005), few studies have quantified the relationship between predicted flood inundation extent (common called top width in engineering analysis) and storm event return interval for surveyed cross sections compared to LiDAR-derived cross sections. This work is an attempt to address this understudied topic to better understand the potential errors introduced when LiDAR is used in place of surveyed data for geometric representation in HEC-RAS. The study is performed on an approximately 6.6 km case study stream reach located in the North Carolina Piedmont. The two overarching research questions addressed in this paper are:

(a) *How do top widths predicted using geometry input derived from LiDAR differ from top widths predicted using traditional surveyed data?*

(b) *Is there a relationship between differences in top width predictions and storm return interval?*

Previous Work

Nearly a decade of research has been conducted on the use of LiDAR for deriving topographic descriptions for hydrologic and hydraulic modeling. Marks and Bates (2000) reported in one of the first papers on the topic that, while LiDAR offered the potential to more accurately quantify topography and topographic change through repeat measurements, the density of the LiDAR response includes significant redundancy and, at the time, interpolation methods for reducing the data volumes were insufficient for use with numerical models. Many researchers have worked to address the data reduction challenge in using LiDAR for hydrology and hydraulic modeling. Two examples of this work are Bates at al. (2003), which proposed methods to optimize the assimilation of LiDAR data into numerical models, and Raber et al. (2007), which investigated the relationship between LiDAR post spacing and the accuracy of floodplain maps to understand the appropriate resolution for LiDAR generated DEMs.

In addition to questions of optimal data reduction techniques, researchers have also investigated the sources and magnitudes of error introduced through the LiDAR data collection process, and have suggested ways in which these errors may impact flood prediction accuracies. Sources of uncertainty introduced through LiDAR data include instrument calibration, missing data, and data filtering algorithms that extract bare earth points from LiDAR point clouds (French 2003; Zhang et al. 2003). Hodgson and Bresnahan (2004) developed an error budget associated with the use of LiDAR for deriving elevations and found that system errors were the dominate source for errors followed by interpolation, horizontal displacement, and surveyor errors. They defined system errors as factors related to the accuracy of the equipment used to collect the data and the data processing algorithms used to derive DEMs from raw LiDAR data. Merwade et al. (2008) identified terrain uncertainty as one of the primary sources of uncertainty introduced in flood inundation modeling, and the authors showed that even slight uncertainties in terrain estimations can lead to uncertainties in the predicted flood inundation extent.

The larger question of the accuracy of topography as stored in digital elevation model grids has also been widely discussed in literature. Prior to the application of LiDAR as a technology for parameterizing flood models, Walker and Willgoose (1999) compared existing DEMs with resolutions of 6.25, 12.5, and 25.0 meters with ground surveys and studied the implications of the differences on hydrologic properties such as width functions, slope-area and cumulative area relationships. They found properties such as cumulative area relationships and width functions to be poorly estimated by DEMs with coarse resolution, while slope-area was less sensitive to DEM spacing. Wang and Zheng (2005) and Sanders (2007) likewise studied the accuracy of inundations based on different available DEM resolutions, but extended their work to also include remote sensing products including LiDAR. This work focused on the sensitivity of flood model predictions to DEM resolution and found LiDAR to be more accurate than the National Elevation Dataset and other available DEMs that generally overestimated flood extents. Cobby et al. (2003) described methods for improving a two dimensional flood model by decomposing the model's finite-element mesh to reflect floodplain vegetation features. They used an image segmentation system that converts the LiDAR height image into separate images of surface topography and vegetation height. Use of the decomposed mesh allowed for better representation of the observed flood extent and prediction of velocity variations in the vegetation features areas, which are of use in predicting localized erosion and deposition patterns. Finally, Tate et al. (2002) demonstrated a technique for combining digital elevation models (DEMs) with surveyed cross sections to create a more accurate geometric representation for floodplain modeling.

While the topic of DEM resolution for flood modeling has been well studied, less work has been conducted on understanding how flood predictions vary for surveyed cross sections compared to cross sections based on remotely sensed DEMs. Thus, the primary objective of this study is to examine the differences in the flood inundation predictions between LiDAR-derived and survey-derived geometry files for storms with different return intervals. This research is important because quantification of the differences between the surveyed and LiDAR-derived geometries on hydraulic modeling has direct impact on the presumption that LiDAR data provides an appropriate surrogate for traditional surveyed cross sections. One potential outcome of this work is to provide guidance regarding potential errors introduced when remotely sensed data is used in place of in-situ surveying for representing channel geometries in flood mapping and hazard management applications.

Methodology

The research questions outlined in Section 1 are addressed through a case study where HEC-RAS is used to model a river reach represented with three different cross section geometries: (1) surveyed geometries, (2) LiDAR derived geometries, and (3) a hybrid of surveyed and LiDAR derived geometries. The model is used to simulate the maximum flood inundation extent for four different storm events (10-year, 50-year, 100-year and 500-year) under steady flow conditions. All other parameters and conditions of the three models are held constant to isolate the impact of channel representation on top width predictions.

Equations for Flood Simulation

The basic computational algorithm of HEC-RAS for steady flow conditions is based on the solution of the one-dimensional energy equation (Equation 1). Water surface profiles are computed in an iterative procedure (the standard step method) that solves the energy equation for each cross section (HEC 2002). The Energy equation is given as

$$y_2 + z_2 + \frac{\alpha_2 V_2^2}{2g} = y_1 + z_1 + \frac{\alpha_1 V_1^2}{2g} + h_e \qquad (1)$$

where y is the depth of water at a cross section, z is the bed elevation of the main channel, v is the average velocity at the cross section, α is the velocity weighting coefficient, g is the gravitational acceleration constant, and h_e is the energy head loss.

The energy head loss term (h_e) is modeled by HEC-RAS as the sum of a friction loss term and a contraction or expansion loss term that accounts for river obstructions such as bridges and culverts. The energy head loss is calculated using Equation 2

$$h_e = L\bar{S}_f + C\left|\frac{\alpha_2 V_2^2}{2g} - \frac{\alpha_1 V_1^2}{2g}\right| \qquad (2)$$

where L is a discharge weighted reach length, $\bar{S}_f$ is a representative friction slope between locations one and two on the stream reach, and C is an expansion or contraction loss coefficient.

Velocity is related to channel conveyance and the friction slope according to Manning's Equation (Equation 3)

$$Q = KS_f^{\frac{1}{2}} \tag{3}$$

where Q is discharge and K is the conveyance term. Conveyance is a function of the channel geometry and the flow depth, as shown by Equation 4

$$K = \frac{1.486}{n} AR^{\frac{2}{3}} \tag{4}$$

where n is Manning's roughness coefficient, A is the flow area, and R is the hydraulic radius. R is calculated as A/P where A is the channel cross-section area and P is its wetted perimeter, both of which are dependent on the channel geometry.

The computation algorithm used in HEC-RAS to solve this system of equations for the water surface elevation is to (1) assume a water surface elevation (y_1), (2) calculate K and V based on the assumed water surface elevation, (3) solve for $\bar{S}_f$ and then h_e using Equation 2, (4) compute y_1 using Equation 1, and (5) repeat steps 1-4 using the result from step 4 as the assumed water surface elevation in step 1 until the water surface calculated in step 4 converges on the water surface elevation assumed in step 1. This study is primary concerned with predicting top width, which can be calculated from the water surface depth given the channel geometry.

Complications to this algorithm arise when flow conditions pass from supercritical flow to subcritical flow or from subcritical flow to supercritical flow. For these situations, the model uses the full momentum equations for fluid flow to solve for the water surface elevation instead of the energy equation discussed here. These transitions can occur with obstructions such as bridges or stream confluences, or with significant changes in the bed slope. A complete description of the mathematics solved in HEC-RAS is available in the HEC-RAS Reference Manual (HEC 2002).

Experiment Design

The overarching objective of this study is to estimate top width for different storm event return intervals and for the three identified geometric representations: (1) survey, (2) LiDAR and (3) hybrid. This experiment is designed to quantify the differences in top width predictions to measure the sensitivity of the model to geometric representation. It is not possible to perfectly describe the channel geometries for the case study reach. Therefore one can only quantify relative errors (which we will call differences in this paper) between two measurement methods. That said, it is assumed that the surveyed channel representation is the "true" channel representation, because this is the *de facto* method used in flood mapping, and so the LiDAR channel representations are compared to the surveyed geometry.

Three statistics are used to quantify the difference between top width predictions. The mean difference (Equation 5) provides a measure of the average deviation of the predicted top width for all cross sections within the model and is calculated as

$$difference = \frac{\sum_{i=1}^{n}(TW_{0,i} - TW_{1,i})}{n} \tag{5}$$

where $TW_{0,i}$ is the top width prediction using the surveyed geometry for the i^{th} cross section and $TW_{1,i}$ is the top width prediction using either the LiDAR or the hybrid geometry for the i^{th} cross section. The mean absolute difference (Equation 6) considers only the magnitude of difference between the top width predictions.

$$difference_{abs} = \frac{\sum_{i=1}^{n} \left| TW_{0,i} - TW_{1,i} \right|}{n} \tag{6}$$

Finally, the Root Mean Square Error (RMSE) (Equation 7) is a commonly used measure for model accuracy and quantifies the spread between the top width predictions for different geometry files.

$$RMSE = \sqrt{\frac{\sum_{i=1}^{n} (TW_{0,i} - TW_{0,i})^2}{n}} \tag{7}$$

These three statistics were calculated for each individual rainfall event as well as for all rainfall events combined. The difference statistics give a direct assessment of the relative difference between inundation predictions between the three models and can be used to assess whether LiDAR-based geometries are over or under predicting the top width compared to survey-based geometries. Thus, these statistics are presented and analyzed in light of the research questions presented in Section 1.

Study Area

The study area used for this analysis is Crooked Creek, a headwater stream located in western Durham County in the Piedmont region of North Carolina (Figure 1). Crooked Creek has a watershed area of approximately 12.4 square km (4.8 square miles) and is a tributary of the

Eno River and then the Neuse River before flowing into the Pamlico Sound. While the area immediately adjacent to the stream is mostly wooded, the watershed contains several developments and road crossings. The land use in the watershed is approximately 60% forest, 30% developed, 9% pastures, cultivated areas and grass lands, and less than 1% open water and woody wetlands, according to the 2001 National Land Cover Dataset (Homer et al. 2007).

Analysis

Two different sources of terrain data were acquired for this study. First, the surveyed cross sections used by the State of North Carolina to generate their FEMA Flood Insurance Rate Map (FIRM) were obtained. These cross sections were available as part of a HEC-RAS model that also included the channel obstructions, hydrologic and hydraulic parameters, and boundary conditions for the HEC-RAS model. Sixty-nine cross sections and nine obstructions (culverts and bridges) were used to model the creek in HEC-RAS (Figure 2). Figure 2 also shows the simulated 100 year flood based on predictions using the LiDAR geometry data. Second, a 6.1-m (20-ft) resolution LiDAR-derived DEM developed by the North Carolina Flood Modernization Program NCFMP was obtained and, for the same cross section locations in the State's HEC-RAS model, a second set of cross section elevations were generated by using HEC-GeoRAS to extract elevation values from this LiDAR-based DEM (HEC 2005).

The two topographic data sources where used to generate three input geometry files for HEC-RAS: (1) surveyed, (2) LiDAR, and (3) hybrid. The surveyed geometry was taken directly from North Carolina's HEC-RAS model. The LiDAR-based geometry input file was generated using HEC-GeoRAS where LiDAR estimations of elevation were extracted along the surveyed cross section to create a new input geometry file. The location of the channel centerline in the

LiDAR geometry was identified using hydrologic terrain processing tools available in the ArcGIS Spatial Analyst Extension (Kopp 1998), while the banks were estimated based on the shape of the cross section. The hybrid file was created by using the elevations extracted from the LiDAR data and the surveyed geometry for the channel bank locations. Figure 3 presents an illustration of the hybrid data combination.

The primary reason for creating the hybrid dataset was to enforce channel back locations at culverts. When a culvert is modeled in HED-RAS, the geometry describing the culvert flow area is contained within the cross sections directly upstream and downstream of that culvert. If the sources of the geometry data used to describe the culvert geometry and location are not in-line with the data used to describe channel cross section locations, this spatial misalignment may cause errors in the hydraulic calculations. The purpose of the Hybrid dataset, therefore, is to test if minimal surveyed data about culvert bank locations significantly improved the LiDAR-based predictions.

Four design storm simulations with seven flow changes along the creek for each simulation were modeled. This inflow data was inserted into the HEC-RAS model at the flow exchange points were developed using the NRCS hydrology methods with Type II rainfall distribution. Table 1 contains a summary of the hydrologic data used in the study to calculate the flow input to the Crooked Creek reach and the sub-watersheds are shown in Figure 2. As previously stated, the other properties of the HEC-RAS model (the obstructions, hydrologic, and hydraulic parameters) were held constant so that the effect of the geometric representation could be quantified. Further, to assure that the top width results were not affected by variations in the locations, lengths, and alignment of the cross sections, these properties were also held constant between the three models. Thus, the sole change between the three models is the source of the geometric data (i.e. cross sections and channel bank locations).

The outputs generated by the HEC-RAS simulations for steady flow conditions include water surface elevation, velocity, flow area, top width, and flow depth. This study focused on analysis of top width, which is a measure of the maximum flood inundation resulting from a storm event. Given that there are sixty-nine cross sections in Crooked Creek and the analysis considered four storm return periods, the total number of top width predictions for each geometric representation is 276 (sixty-nine multiplied by four). Flood prediction comparisons were conducted by calculating the difference, absolute difference, and the Root Mean Square Error (RMSE) as discussed in a previously.

Results and Discussion

The comparison statistics of the top width predictions for hybrid versus survey and LiDAR versus survey are presented in Table 2. There are a number of important points that can be drawn from these statistics. First, the results show a negative correlation between both average difference and average absolute difference with respect to return period. The largest difference in the top width predictions occurs for the 10-Year event (18% average absolute difference with a range of 0.1% to 64% for the LiDAR dataset and 15.5% with a range of 0.1% to 31% for the Hybrid dataset). The average absolute difference then decrease as the return period increases, to approximately 12.5% (range of 0.2% to 33%) for 50 and 100 year events, to below 10% (range of 0.1% to 31%) for the 500 year event. Second, average difference is always positive, indicating that the simulation using the hybrid and LiDAR geometries predicted higher top width values compared to the simulations using the survey geometry. Third, the hybrid dataset consistently outperforms the LiDAR dataset by 1-3% in terms of average absolute difference and 2-4% in terms of average difference. Finally, the RMSE statistic interestingly does not show a strong relationship with return period, decreasing slightly in magnitude for the 10 to 50 year events, but then increasing slightly for the 100 and 500 year events. Perhaps the most important point, however, is that, based on these results, the LiDAR dataset produces top width estimations that are approximately 7% greater than predictions based on a surveyed dataset for large storms (500 year return interval) and over 11% greater for small storms (10 year return interval).

In order to examine differences in the top width predictions, the LiDAR and survey cross section plots were visually examined. The survey and LiDAR cross sections appeared to generally match, despite some disagreements. Figure 4 presents an example of the top width and water surface elevation predictions at the two cross sections: one where the surveyed and LiDAR-derived cross sections generally match, and one where there was significant disagreement between the two cross-sections. In the first case where there was a good match between the survey and LiDAR-based cross sections, the survey-based top width prediction was 110.4 m and the LiDAR-based top width prediction was 120.8 m (a 9.4% difference). Both models in this first case predicted a maximum water surface elevation of 129.0 m. In the second case where there is a poor match between the cross sections, the survey-based top width prediction was 96.7 m and the LiDAR-based top width prediction was 109 m (a 12.7% difference). In this second case, the survey-based model predicted a maximum water surface elevation of 136.7 while the LiDAR based model predicted a water surface elevation of 136.4 m.

A closer examination of the prediction differences relieved a pattern where cross sections directly upstream or downstream of road crossings had the greatest absolute differences. Comparing the surveyed and LiDAR-derived cross sections for all road crossings revealed that the cross sections often match either the upstream or downstream sides of a road crossing, but never for both. Figure 5 provides an example of cross section duplication at Bramble Drive crossing of Crooked Creek. The solid line in the cross section plot represents the surveyed cross section and the dashed line the LiDAR-based cross section. Interestingly, the surveyed cross sections are identical for both the upstream and downstream cross sections after taking into account a 0.07 m (0.2 ft) vertical shift. Thus, it appears that the surveyed cross section represented in the HEC-RAS model is in fact the upstream cross section, and that this cross section was duplicated to create the downstream cross-section. Because of the high cost of collecting surveyed cross sections and time constraints, we suspect that the modeler assumed terrain conditions were constant on both sides of a road crossing and duplicated cross sections. Nonetheless, this analysis highlights one potential use for LiDAR data: not necessarily to create cross section data themselves, but as a means for validating cross sections within existing HEC-RAS models.

Table 3 presents the percent differences in top width predictions for the cross sections upstream and downstream of the Bramble Drive crossing. The differences for the upstream cross section show a weak correlation with return period. The differences increase from approximately 13% for the 10 and 50 year return interval to over 20% for the 100 and 500 year return interval. On the other hand, the differences for the downstream cross sections show a consistent trend with the overall difference pattern, that is a negative correlation with return period. The LiDAR and hybrid set are under-predicting the top width by 63% for the 10 year return event, the difference decreases in magnitude with increasing return interval to 8.5% and 4.9% for the hybrid and LiDAR datasets, respectively for the 500 year . Based on plots of the cross sections for the upstream and downstream ends of this cross section, we know that the surveyed cross section downstream of the road crossing was incorrectly accounted for in the model. At the same time, the road crossings are flow control points within the hydraulics model where flow is constricted or expanded through the system, complicating the hydraulics and potentially increasing the differences. Depending on the culvert or bridge's capacity, the top width will change significantly for varying flows. Therefore, having accurate culvert and cross section information at road crossings is essential for an accurate top width prediction at those locations.

Given the observation of duplicate cross sections, the statistics previously calculated for the entire population of cross sections were recalculated for three subsets of the overall cross section dataset: (1) a subset that excluded all road crossing cross sections, (2) a subset that included only road crossings' upstream cross sections, and (3) a subset that included only road crossings' downstream cross sections. Of the sixty-nine cross sections used in this analysis, eighteen represent cross sections associated with road crossing. Table 4 presents the difference statistics for the population excluding the road crossing cross sections, while Tables 5 and 6 presents the difference statistics for only upstream and downstream cross sections respectively. The statistics presented in Table 4 indicate that, after excluding road crossings, the difference between surveyed and LiDAR-based cross sections decreased by 3-5% for average absolute difference and 1-3% for average difference. The RMSE statistic, while being generally unrelated to return period when considering the overall population of cross sections, now shows a negative correlation with return period after removing the cross sections associated with road crossings. This reduction in errors is illustrated in Figure 6. Based on the RMSE statistic, top width predictions were between 4.8 m (15.7 ft) (for a 500 year event) and 8.1 m (26.6 ft) (for a 10 year event) different when comparing the LiDAR-based data with the surveyed data. Also for

LiDAR, the average absolute difference drops to 11% for a low flow event (10 year return period) and below 5% for a major storm event (500 year return period). Considering only cross sections at road crossings (Tables 5 and 6), the data shows that all three difference statistics are much higher than the differences associated with the entire population and there is no correlation between the differences and the return period.

The results were summarized into a Cumulative Distribution Function (CDF) for the probability that a cross section's error exceeds some value *a* (Figure 7). The top graph is the CDF for the LiDAR absolute difference, it shows that the probability of a cross section having a difference less than or equal to 10% is 57% for a 10 year event, 67% for a 50 year event, 71% for a 100 year event, and 75% for a 500 year event. Excluding the cross sections associated with road crossings, the probability that the difference at a given cross section is less that 10% increases from 68% to 80%. The CDF for the hybrid absolute difference shows the same general trend, with the probabilities being 54% for a 10 year event, 59% for a 50 year event and 62% for a 100 year event, and 70% for a 500 year event. The probabilities increase from 62% to 72% after removing cross sections associated with road crossings. Figure 7 also shows that the CDFs associated with each storm event tend to converge as the probability increases, with the exception of the 10 year storm event. For example, there is a 10% chance of having a 50% or higher difference for a 10 year event, while all other storm events have less than a 5% chance of exceeding a 50%difference. This confirms the finding that the difference between LiDAR and surveyed cross sections is most significant for low flow events.

Conclusions

The results of the study show that top width predictions generated using LiDAR-based cross section geometries generally overestimate predictions generated using survey-based geometries. The average difference ranged from 6% for the 500 year event to 12% for the 10 year event, and the average absolute difference ranged from 6% for a 500 year event to 14% for a 10 year event. When comparing LiDAR-based cross sections with hybrid-based cross sections, this study found that the hybrid-based cross sections produced top width predictions more similar to survey-based cross sections. The hybrid dataset used LiDAR data for the cross section elevations and the surveyed data for locating the channel banks.

The study showed greater differences associated with the cross sections directly upstream and downstream of the road crossings. Graphical exploration of these cross sections revealed that only one cross section at each road crossing was actually surveyed, and that surveyed cross section was duplicated for the other side of the road crossing. When comparing the duplicated survey-derived cross sections against LiDAR data, LiDAR often validates the original cross section, but also suggests that the upstream and downstream sides of the road crossings do not have similar geometries. Considering the top width predictions for all design storm events, the differences in top width predictions for LiDAR versus surveyed cross sections decreases from 11% to 7% after the cross sections associated with road crossings were excluded from the analysis. Although greater differences were observed at road crossings, this study was unable to conclude if these differences are a result of the duplication of cross sections in the surveyed dataset, or due to increased hydraulic complexity associated with flow expansions and contractions at road crossings.

Future work is needed to expand the scope of this study to include additional watersheds with varying climates, geomorphology, vegetative cover, and stream-order. This will allow for a better understanding of how such factors influence LiDAR's ability to measure flood plain and channel elevations for flood modeling. Also, this study should be expanded through future research to model historical flood events in order to quantify true instead of relative errors. Such research could be done using a steady-state model where the attempt would be to predict the maximum water surface elevation and top width, or using a unsteady-state event where the attempt would be to model the water surface elevation and top width through time. Quantifying the true errors when compared to a historical event instead of relative errors (or differences) reported in this study will allow for more definite conclusions as to the value of LiDAR compared to survey derived cross sections.

Acknowledgments

This research was funded in part by the Renaissance Computing Institute (RENCI).

References

Bates, P. D., Marks, K. J., and Horritt, M. S. (2003). "Optimal use of high-resolution topographic data in flood inundation models." *Hydrological Processes*, 17(3), 537-557.

Federal Emergency Management Agency (FEMA). (2003). “Guidelines and Specifications for Flood Hazard Mapping Partners, Appendix A: Guidelines for Aerial Mapping and Surveying.” <http://www.fema.gov/pdf/fhm/frm_gsaa.pdf> (Apr. 14, 2008).

Cobby, D.M., Mason, D., Horritt, M.S. and Bates, P.D., (2003). "Two-dimensional hydraulic flood modeling using a finite element mesh decomposed according to vegetation and topographic features derived from airborne scanning laser altimetry.” *Hydrological Processes*, 17 (10), 1979-2000.

French, J.R., (2003). “Airborne LiDAR in support of geomorphological and hydraulic modeling.” *Earth Surface Processes and Landforms*, 28(3), 321-335.

Hodgson, M.E., and Bresnahan, P. (2004). “Accuracy of airborne lidar-derived elevation: Empirical assessment and error budget.” *Photogrammetric Engineering and Remote Sensing*, 70(3), 331-339.

Homer, C., Dewitz, J., Fry, J., Coan, M., Hossain, N., Larson, C., Herold, N., McKerrow, A., VanDriel, J. N., and Wickham, J. (2007). "Completion of the 2001 National Land Cover Database for the conterminous United States." *Photogrammetric Engineering and Remote Sensing*, 73(4), 337-341.

HEC (Hydrologic Engineering Center), (2002). “HEC-RAS, River Analysis System.” Hydraulic Reference Manual. HEC. http://www.hec.usace.army.mil/software/hec-ras/documents/HEC-RAS_4.0_Reference_Manual.pdf> (Nov 5, 2008).

HEC (Hydrologic Engineering Center), (2005). “HEC-GeoRAS, GIS Tools for support of HEC-RAS Using Arc-GIS.”, User’s Manual, Version 4. < http://www.hec.usace.army.mil/software/hec-ras/hec-georas.html >

IPCC (The International Panel on Climate Change), (2001). "IPCC WGI, Climate change 2001: the scientific basis, contribution of working group I to the third assessment report of the Intergovernmental Panel on Climate Change (IPCC)." In: J.T. Houghton, Y. Ding, D.J. Griggs, M. Noguer, P.J. van der Linden and D. Xiaosu, Editors, Cambridge University Press, UK, 944 p.

Kopp, S. (1998). "Developing a Hydrology Extension for ArcView Spatial Analyst." *Arc User*, ESRI, 18-20.

Marks, K., and Bates, P. (2000). “Integration of high-resolution topographic data with floodplain flood models.” *Hydrological Processes*, 14(11-12), 537-557.

Merwade, V., Olivera, F., Arabi, M., and Edleman, S. (2008a). "Uncertainty in flood inundation mapping: Current issues and future directions." *Journal of Hydrologic Engineering*, 13(7), 608-620.

NAS (National Academy of Science), (2007).” Elevation Data for Floodplain Mapping.” *National Academies Press*, 500 Fifth Street, NW, Washington, D.C. 20001.

NCFPM (North Carolina Floodplain Mapping Program), (2003). “Issue 37: Quality Control of Light Detection and Ranging Elevation Data in North Carolina for Phase II of the North Carolina Floodplain Mapping Program.” <http://www.ncfloodmaps.com/pubdocs/issue_papers/IP37-phaseII_lidar_qc.pdf> (Apr. 23, 2008).

Raber, G.T., Jensen. J.R., Hodgson, M.E., Tullis, J.A., Davis, B.A., and Berglund, J. (2007). "Impact of Lidar Nominal Post-spacing on DEM Accuracy and Flood Zone Delineation." *Photogrammetric Engineering & Remote Sensing*, 73(7), 793–804.

Sanders, B.F. (2007). "Evaluation of on-line DEMs for flood inundation modeling." *Advances in Water Resources*, 30 (2007), 1831–1843.

Shamsi, U.M. (2001). "GIS and Modeling Integration." *CE News*, 13(6), 46-49.

Tate, E. C., Maidment, D. R., Olivera, F., and Anderson, D. J. (2002). "Creating a terrain model for floodplain mapping." *Journal of Hydrologic Engineering*, 7(2), 100-108.

USACE and FEMA. (2000). "Hurricane Floyd assessment: Review of hurricane evacuation studies utilization and information dissemination." Post, Buckley, Schuh and Jernigan, Inc., Tallahassee, FL, < http://www.csc.noaa.gov/hes/docs/postStorm/_H_FLOYD_ASSESSMENT_ REVIEW_HES_UT ILIZATION_INFO_DISSEMINATION.pdf > (Nov. 5, 2008)

Walker, J.P., and Willgoose, G.R. (1999). "On the effect of digital elevation model accuracy on hydrology and geomorphology." *Water Resources Research*, 35(7), 2259-2268.

Wang, Y., and Zheng, T. (2005). "Comparison of Light Detection and Ranging and National Elevation Dataset Digital Elevation Model on Floodplains of North Carolina." *Natural Hazards Review*, 6(1), 34-40.

WMO (World Meteorological Organization), 2003 "Our Future Climate." Publication WO-952.

Zhang, K.Q., Chen, S.C., Whitman, D., Shyu, M.L., Yan, J.H., and Zhang, C.C. (2003). "A progressive morphological filter for removing nonground measurements for airborne LIDAR data." *IEEE Transactions On Geoscience and Remote Sensing*, 42(4), 872-882.

Captions

Table 1. Summary of the steady flow hydrologic input data

Table 2. Comparative statistics for the variations in top width predictions using the entire cross section population

Table 3. Error in top width predictions for the cross sections immediately upstream and downstream of Bramble Drive crossing

Table 4. Comparative statistics for the variations in top width predictions excluding the cross sections associated with road crossings

Table 5. Comparative statistics for the variations in top width predictions for the cross sections upstream of the road crossings

Table 6. Comparative statistics for the variations in top width predictions for the cross sections downstream of the road crossings

Figure 1. Crooked Creek in Durham County, North Carolina

Figure 2. Crooked Creek cross sections, sub-watersheds and 100 YR flood delineation

Figure 3. Illustration of the hybrid data combination

Figure 4. Graphical comparison of the Survey and DEM cross sections. (top: high agreement, bottom: high disagreement) and the 100 YR flood delineations

Figure 5. Duplicate cross sections used in the original model for the upstream and downstream cross sections at Bramble Drive crossing.

Figure 6. Error statistics of the top width predictions using the entire cross section population and the population excluding cross sections associated with road crossing

Figure 7. Cumulative distribution function (CDF) of average absolute error for the LiDAR (top) and hybrid (bottom) cross section datasets

Table 1

Basin ID	Sub-Basin Area (km^2)	Basin Area (km^2)	Final Discharges (m^3/sec)			
			Q10	Q50	Q100	Q500
CC1	2.75	2.75	34.32	49.36	58.39	81.52
CC2	0.26	2.98	31.80	50.74	60.03	83.39
CC4	0.23	5.62	44.00	66.60	82.09	125.90
CC6	0.57	7.33	45.59	71.50	90.44	139.49
CC7	3.03	10.36	73.54	106.50	128.95	183.72
CC8	1.22	11.58	79.68	114.06	137.00	193.40
CC9	0.88	12.48	78.04	120.60	145.63	205.41

Table 2

Rainfall (mm)	Return Period of Rainfall Event	RMSE (m)		AVG. Absolute Difference (%)		AVG. Difference (%)	
		LiDAR	Hybrid	LiDAR	Hybrid	LiDAR	Hybrid
141	10 Years	12.91	11.99	17.97	15.51	11.02	7.07
178	50 Years	11.33	10.89	12.62	10.86	8.15	4.41
199	100 Years	12.03	11.36	12.20	10.11	8.61	5.37
254	500 Years	12.06	11.59	9.46	8.22	6.72	4.03

Table 3

Rainfall (mm)	Return Period of Rainfall Event	Percent Difference in the Inundation width at the Upstream Cross Section (16892.8)		Percent Difference in the Inundation width at the Downstream Cross Section (16812.8)	
		LiDAR	Hybrid	LiDAR	Hybrid
141	10 Years	12.57	12.95	-63.50	-63.24
178	50 Years	12.98	21.66	-24.23	-32.58
199	100 Years	21.47	21.10	-11.13	-13.05
254	500 Years	21.47	20.04	8.52	4.93

Table 4

Rainfall (mm)	Return Period of Rainfall Event	RMSE (m)		AVG. Absolute Difference (%)		AVG. Difference (%)	
		LiDAR	Hybrid	LiDAR	Hybrid	LiDAR	Hybrid
141	10 Years	9.54	8.11	13.58	10.79	11.73	6.84
178	50 Years	6.43	5.37	8.49	6.30	7.17	2.85
199	100 Years	6.82	5.06	8.42	5.81	7.02	2.89
254	500 Years	5.58	4.79	6.01	4.69	4.13	0.96

Table 5

Rainfall (mm)	Return Period of Rainfall Event	RMSE (m)		AVG. Absolute Difference (%)		AVG. Difference (%)	
		LiDAR	Hybrid	LiDAR	Hybrid	LiDAR	Hybrid
141	10 Years	19.64	19.61	29.74	29.52	24.55	24.15
178	50 Years	22.49	22.33	24.56	24.19	19.37	18.70
199	100 Years	25.08	24.78	25.26	24.32	19.70	22.36
254	500 Years	20.70	20.57	15.89	16.02	12.55	12.93

Table 6

Rainfall (mm)	Return Period of Rainfall Event	RMSE (m)		AVG. Absolute Difference (%)		AVG. Difference (%)	
		LiDAR	Hybrid	LiDAR	Hybrid	LiDAR	Hybrid
141	10 Years	19.38	18.55	31.07	28.22	-6.55	-8.75
178	50 Years	15.60	15.75	24.09	23.30	2.47	-1.01
199	100 Years	14.71	15.14	20.56	20.28	6.48	2.64
254	500 Years	22.58	21.85	22.55	20.44	15.56	12.52

Figure 1

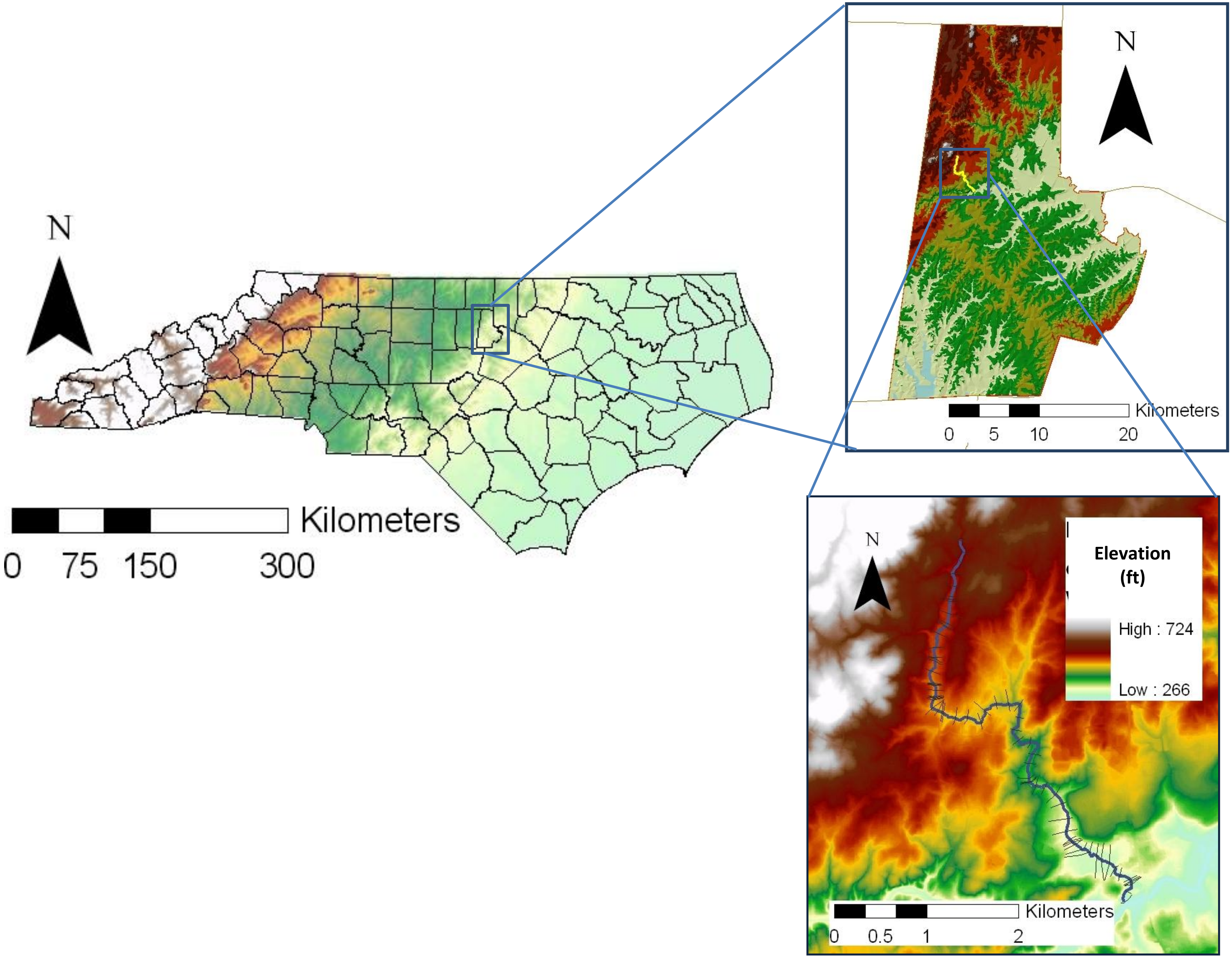
N
Kilometers
0
75
150
300
N
Kilometers
0
5
10
20
N
Elevation (ft)
High : 724
Low : 266
Kilometers
0
0.5
1
2

Figure 2

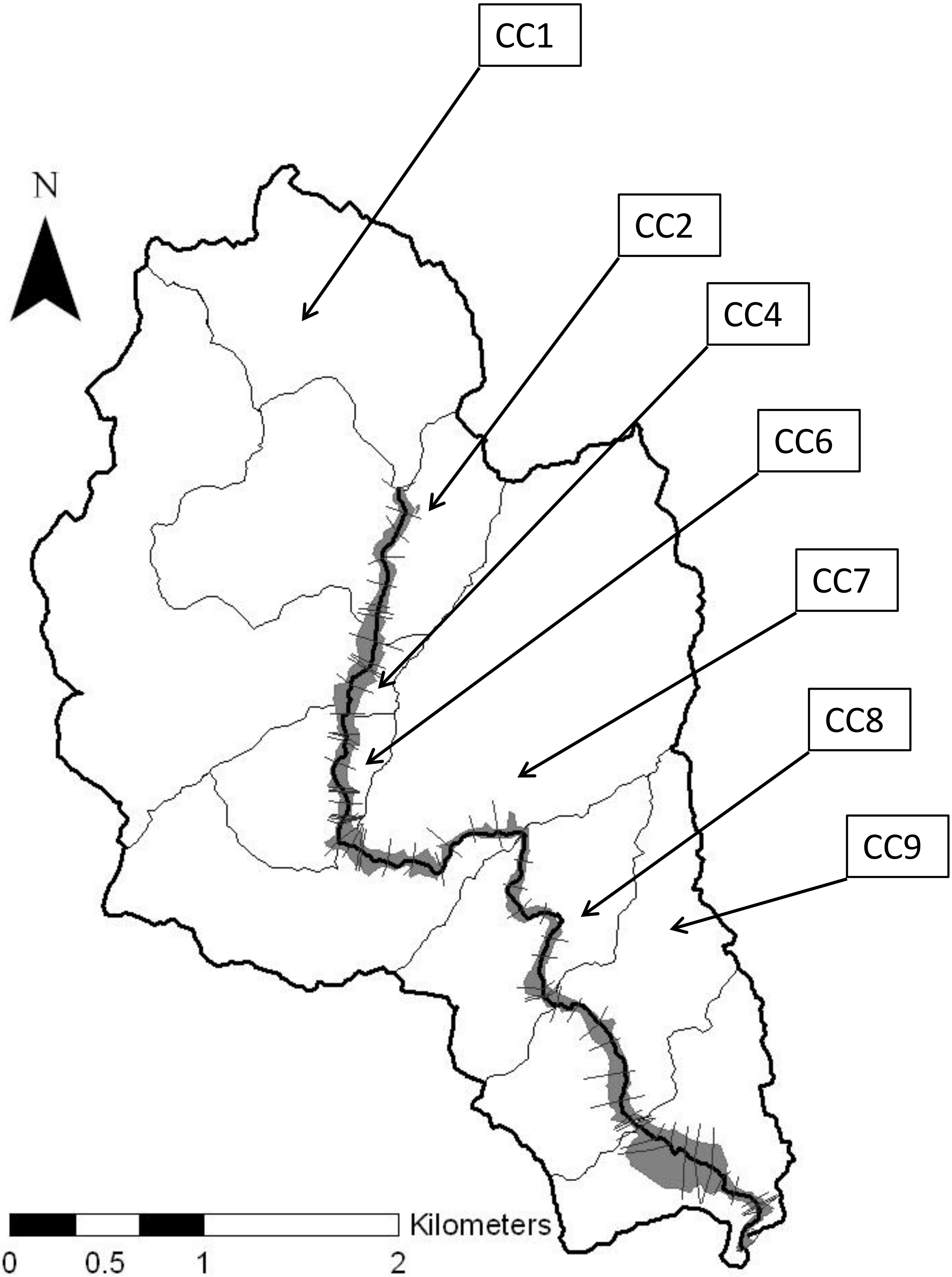

Figure 3

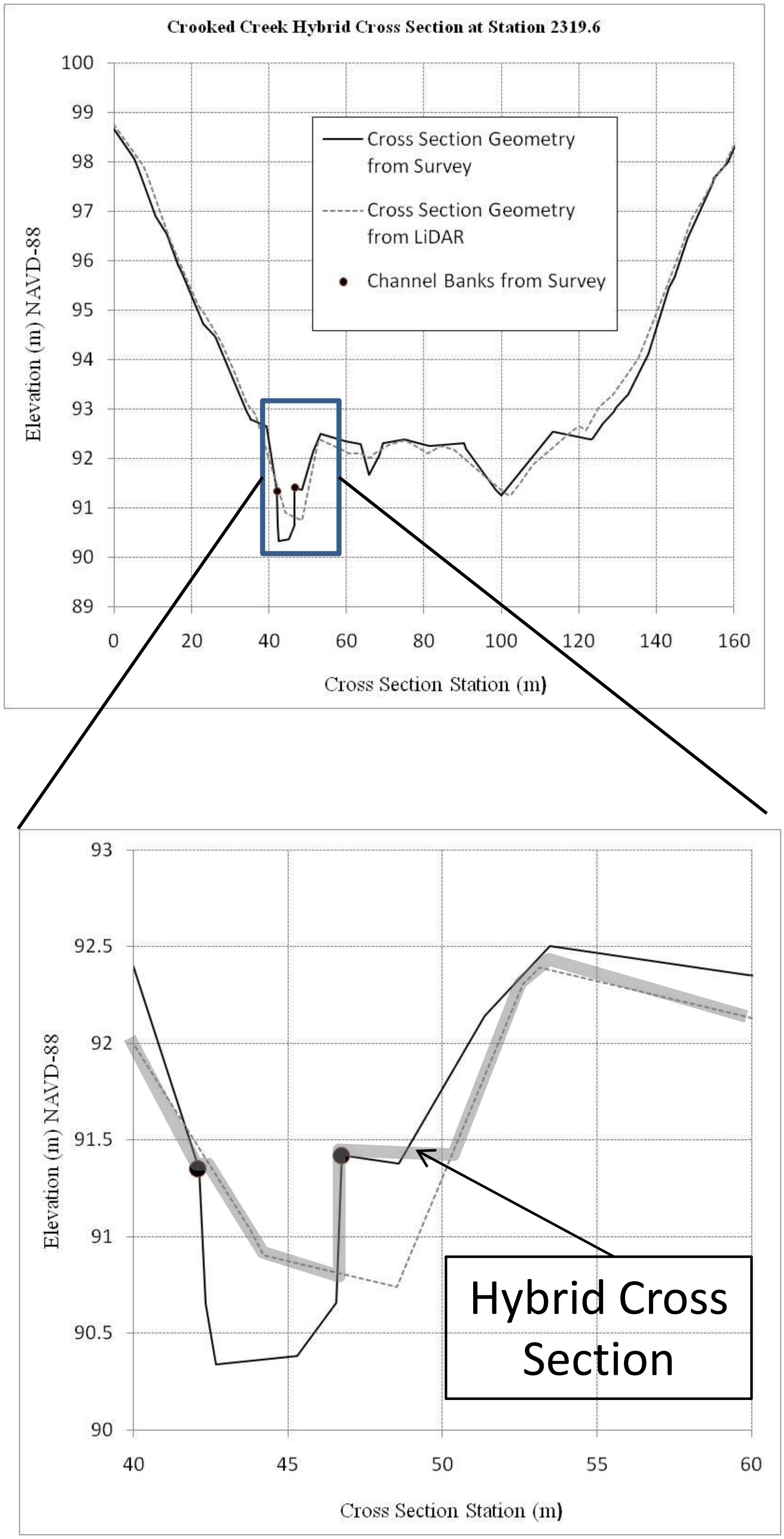

Crooked Creek Hybrid Cross Section at Station 2319.6
Elevation (m) NAVD-88
Cross Section Station (m)
Cross Section Geometry from Survey
Cross Section Geometry from LiDAR
Channel Banks from Survey
100
99
98
97
96
95
94
93
92
91
90
89
0
20
40
60
80
100
120
140
160
Elevation (m) NAVD-88
Cross Section Station (m)
93
92.5
92
91.5
91
90.5
90
40
45
50
55
60
Hybrid Cross Section

Figure 4

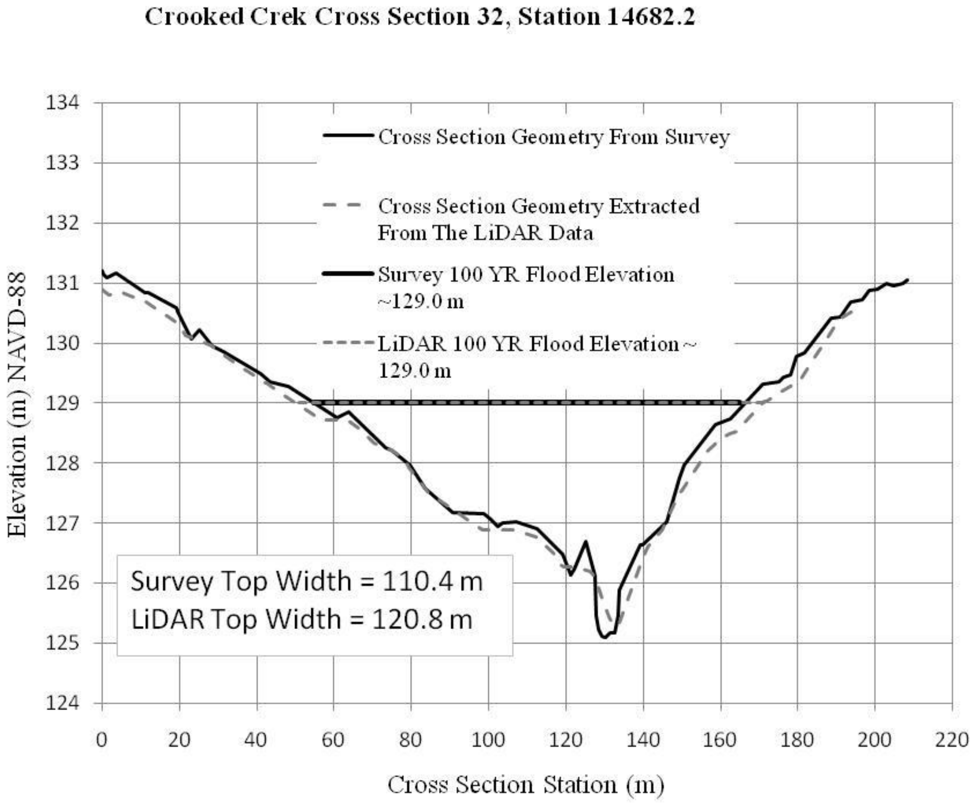

Crooked Crek Cross Section 32, Station 14682.2
Cross Section Geometry From Survey
Cross Section Geometry Extracted From The LiDAR Data
Survey 100 YR Flood Elevation ~129.0 m
LiDAR 100 YR Flood Elevation ~ 129.0 m
Survey Top Width = 110.4 m
LiDAR Top Width = 120.8 m
Elevation (m) NAVD-88
Cross Section Station (m)

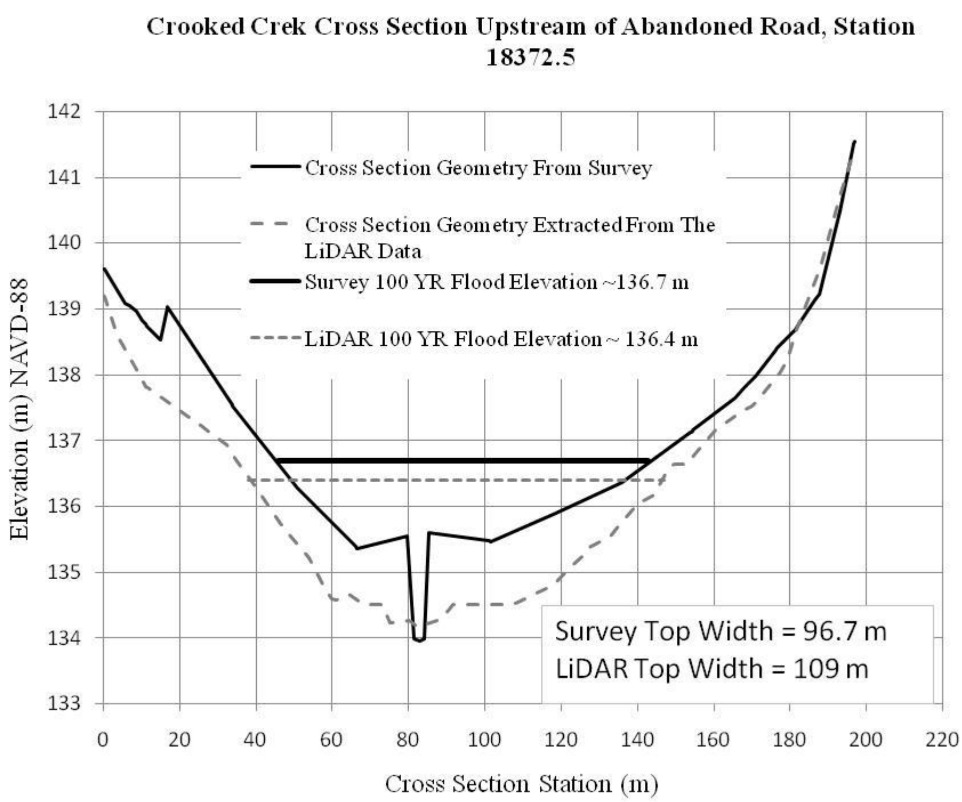

Crooked Crek Cross Section Upstream of Abandoned Road, Station 18372.5
Cross Section Geometry From Survey
Cross Section Geometry Extracted From The LiDAR Data
Survey 100 YR Flood Elevation ~136.7 m
LiDAR 100 YR Flood Elevation ~ 136.4 m
Survey Top Width = 96.7 m
LiDAR Top Width = 109 m
Elevation (m) NAVD-88
Cross Section Station (m)

Figure 5

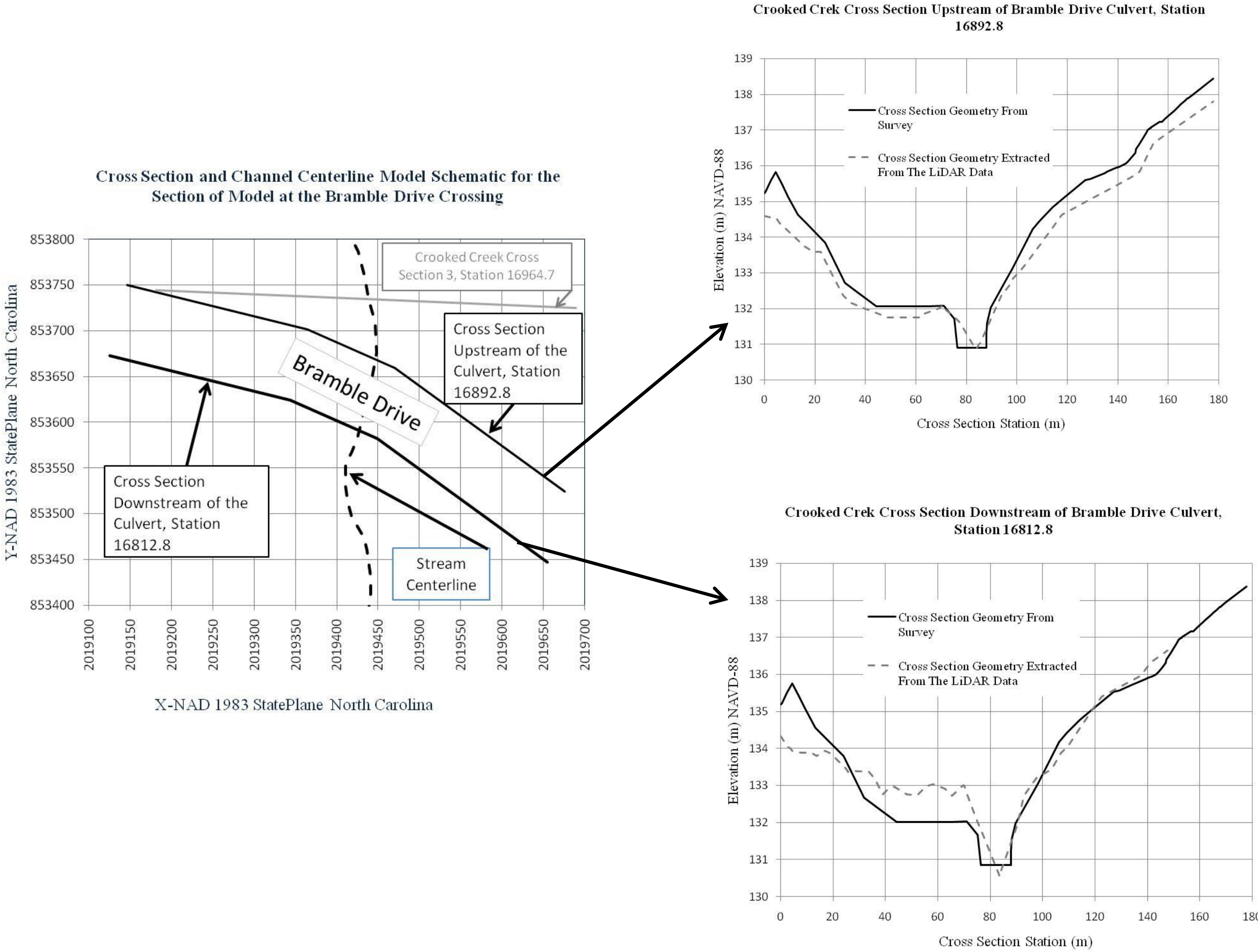

Cross Section and Channel Centerline Model Schematic for the Section of Model at the Bramble Drive Crossing
Crooked Creek Cross Section 3, Station 16964.7
Cross Section Upstream of the Culvert, Station 16892.8
Bramble Drive
Cross Section Downstream of the Culvert, Station 16812.8
Stream Centerline
Y-NAD 1983 StatePlane North Carolina
X-NAD 1983 StatePlane North Carolina
Crooked Crek Cross Section Upstream of Bramble Drive Culvert, Station 16892.8
Cross Section Geometry From Survey
Cross Section Geometry Extracted From The LiDAR Data
Elevation (m) NAVD-88
Cross Section Station (m)
Crooked Crek Cross Section Downstream of Bramble Drive Culvert, Station 16812.8
Cross Section Geometry From Survey
Cross Section Geometry Extracted From The LiDAR Data
Elevation (m) NAVD-88
Cross Section Station (m)

Figure 6

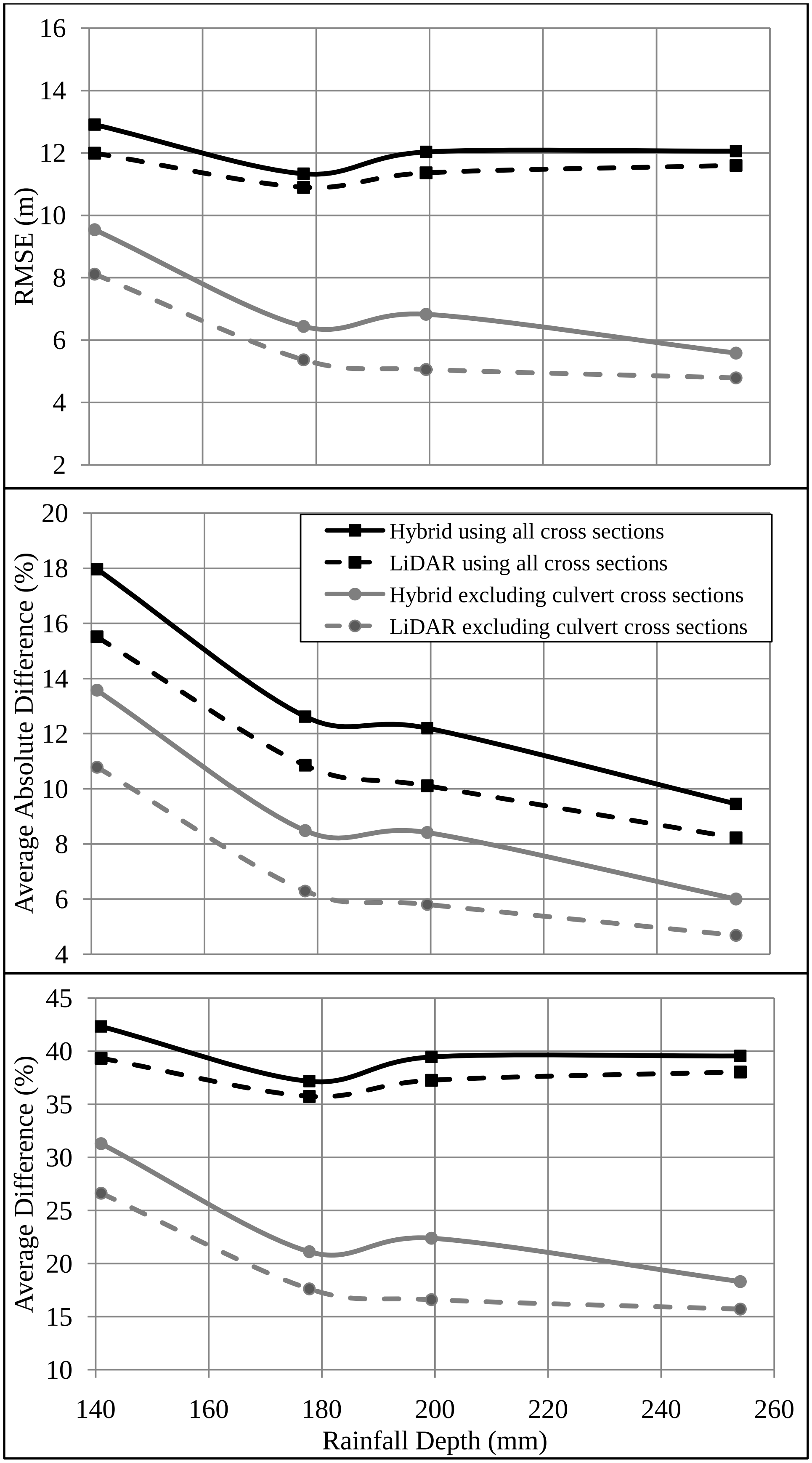
16
14
12
10
8
6
4
2
RMSE (m)
20
18
16
14
12
10
8
6
4
Average Absolute Difference (%)
Hybrid using all cross sections
LiDAR using all cross sections
Hybrid excluding culvert cross sections
LiDAR excluding culvert cross sections
45
40
35
30
25
20
15
10
Average Difference (%)
140
160
180
200
220
240
260
Rainfall Depth (mm)

Figure 7

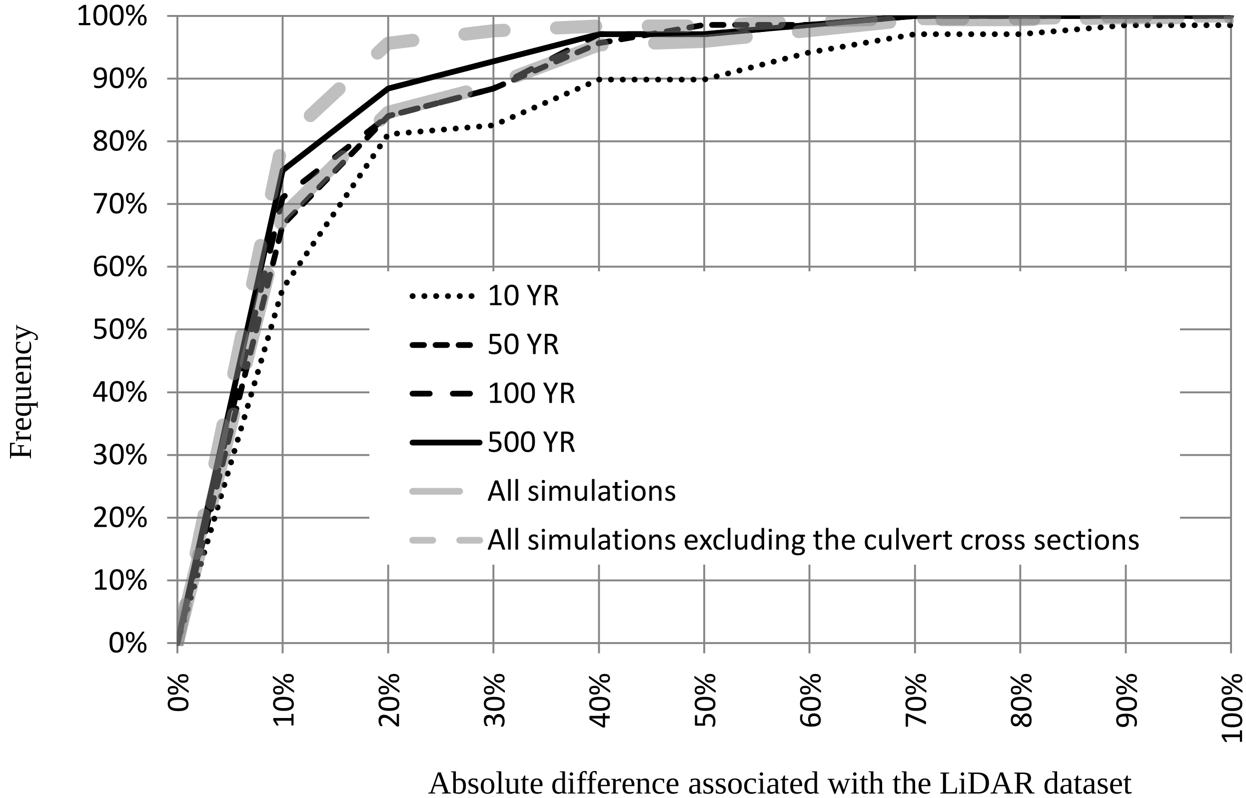
100%
90%
80%
70%
60%
50%
40%
30%
20%
10%
0%
Frequency
10 YR
50 YR
100 YR
500 YR
All simulations
All simulations excluding the culvert cross sections
0%
10%
20%
30%
40%
50%
60%
70%
80%
90%
100%
Absolute difference associated with the LiDAR dataset

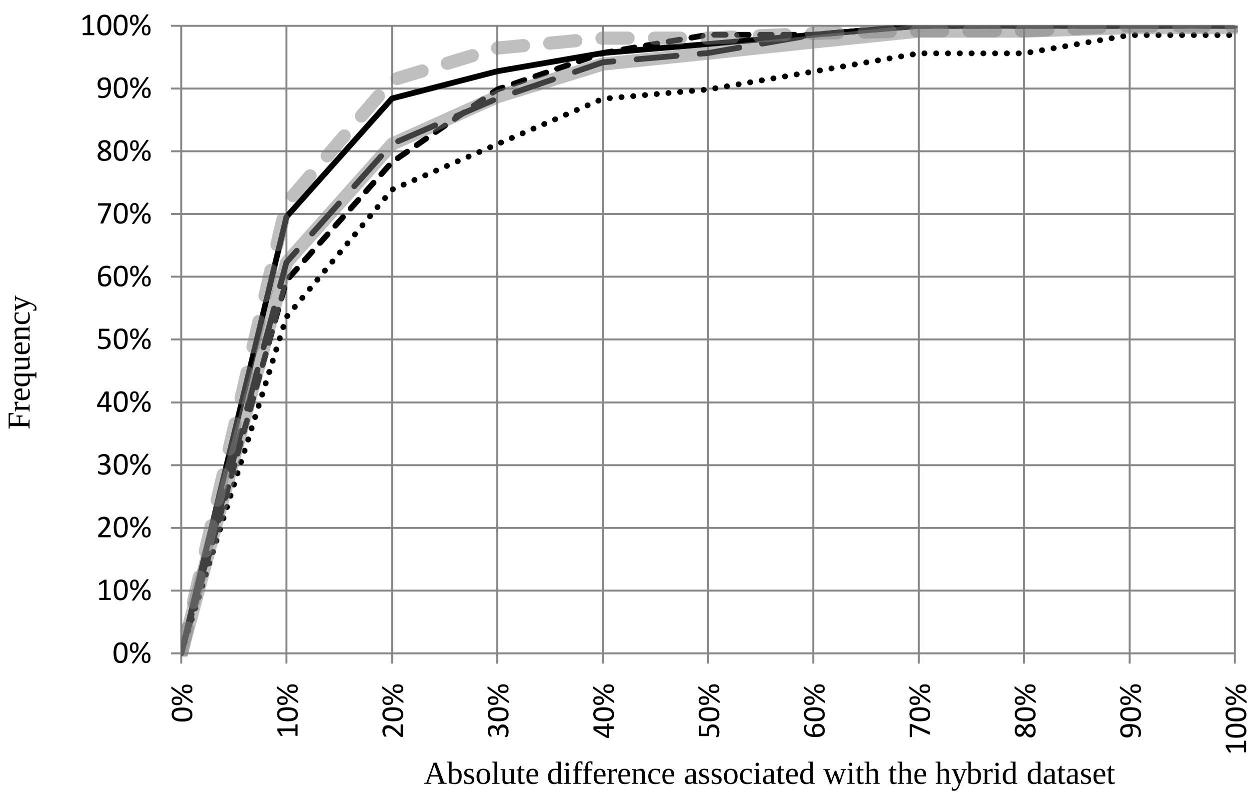
100%
90%
80%
70%
60%
50%
40%
30%
20%
10%
0%
Frequency
0%
10%
20%
30%
40%
50%
60%
70%
80%
90%
100%
Absolute difference associated with the hybrid dataset